

Phase diagram of hole-doped cuprates based on ^{17}O and ^{63}Cu NMR quadrupole splittings

Damian Rybicki^{1,2}, Michael Jurkutat¹, Steven Reichardt¹,
Jürgen Haase¹

¹ University of Leipzig, Faculty of Physics and Earth Sciences, Linnestr. 5, 04103 Leipzig, Germany

² AGH University of Science and Technology, Faculty of Physics and Applied Computer Science, Department of Solid State Physics, al. A. Mickiewicza 30, 30-059 Kraków, Poland

E-mail: rybicki@physik.uni-leipzig.de

Abstract. The phase diagram of the superconducting cuprates is often used to show how their electronic properties change as a function of the mean doping level, i.e., the average hole content of the CuO_2 plane. In Nuclear Magnetic Resonance (NMR) experiments average doping, as well as the distribution of these holes between planar Cu and O reveals itself through the quadrupole splittings of the $^{63,65}\text{Cu}$ and ^{17}O NMR. Here we argue based on all published NMR data available to us in favor a new type of phase diagram that has the planar oxygen quadrupole splitting and with it the planar oxygen hole content as abscissa rather than the average hole content of the CuO_2 plane. In such a plot the superconducting domes of the different cuprate families are shifted horizontally according to their maximum critical temperature $T_{c,\text{max}}$ set by the chemistry of the parent material, which determines its oxygen hole content. The higher the O hole content the higher $T_{c,\text{max}}$ that can be achieved by actual doping. These findings also offer a strategy for finding cuprates with higher $T_{c,\text{max}}$.

PACS numbers: 74.25.nj, 74.72.Gh

Submitted to: *J. Phys.: Condens. Matter*

1. Introduction

The well-known phase diagram of the hole doped high-temperature superconducting cuprates (HTSCs) has at zero doping ($x = 0$) the antiferromagnetic insulator and by increasing x this state disappears rapidly. The so-called "superconducting dome" appears at a few percent of doping, with the superconducting transition temperature T_c reaching its maximum ($T_{c,\text{max}}$) near $x \approx 0.15$ (optimal doping). Further increase of the doping causes a gradual decrease of T_c on the overdoped side. Why $T_{c,\text{max}}$ is so different for different HTSC is not understood. It is believed that the understanding of the various electronic phases that appear to be generic to the different regions of the phase diagram will hold the clue also for understanding $T_{c,\text{max}}$. This believe is not supported by our results discussed below. We will argue, based on all published NMR data available to us, that doping the HTSC only unlocks the $T_{c,\text{max}}$ that is strongly influenced by the parent's hole sharing between planar copper and oxygen. A phase diagram that has the planar oxygen hole content as abscissa, rather than x leads to well-ordered superconducting domes according to their $T_{c,\text{max}}$.

NMR is a powerful local probe that contributed tremendously to the understanding of the chemical and electronic structure of the HTSCs[1]. For example, NMR can measure the electronic spin susceptibility with shift and relaxation measurements, and NMR discovered early on the pseudo-gap above T_c on the underdoped side of the phase diagram, a property markedly different from those of classical superconductors.[2] For many years, it was believed that the shift and relaxation measurements can be understood with a single electronic fluid's spin response. However, with a set of NMR shift experiments at ambient and very high pressures on various systems it was shown, recently, that a single temperature dependent electronic spin component cannot explain the data.[3, 4, 5] Here, we do not discuss the magnetic properties of the HTSC, but address the quadrupole splitting of the NMR of planar Cu and O.

Since $^{63,65}\text{Cu}$ and ^{17}O possess an electric quadrupole moment (nuclear spin $I > 1/2$), the quadrupole interaction gives additional insight into structural details of the HTSCs. In the absence of a magnetic field, the quadrupole interaction splits the degenerate nuclear spin levels, and in a high magnetic field, i.e., where the Zeeman interaction dominates the quadrupole interaction, the latter shifts the levels so that the NMR lines split into $2I$ transitions.[6] The splitting depends on the orientation of the magnetic field with respect to the crystal axes, and from angular dependent studies one can determine the principle axes values and the orientation of the tensor of the electric field gradient (EFG) that interacts with a nucleus' quadrupole moment.

For the electron doped systems there are only few $^{63,65}\text{Cu}$ NMR studies known, and ^{17}O data are lacking, completely. Luckily, the situation is quite different for the hole-doped HTSCs where a large number of studies is available. These show that the quadrupole splittings for both nuclei in the CuO_2 plane depend linearly on the average doping level and thus the total hole content of the CuO_2 plane, and various models including first-principle calculations addressed this observation, e.g. Ref. [7, 8, 9].

Here we investigate all published ^{17}O and ^{63}Cu NMR data accessible to us (collected in Tabs. 1 and 2), and without invoking a special quantitative microscopic model that relates the NMR splitting to the hole content of the various orbitals we arrive at important conclusions. We show that the splittings at both nuclei are very good measures of the doping level, and we argue that different parent materials ($x = 0$) differ in the hole distribution between Cu and O, only. It emerges that $T_{c,\max}$ is set by this distribution such that the bigger the planar O hole content the higher the $T_{c,\max}$. The actual doping only unlocks this potential (probably by destroying the Cu based magnetism). Thus, with respect to the number of O or Cu holes different families of HTSCs occupy very different regions in a phase diagram that has oxygen splitting and with it the number of oxygen holes as abscissa. Here, all HTSCs appear ordered, the higher the oxygen hole content of the parent material the larger $T_{c,\max}$ of that system, irrespective of peculiarities often discussed, e.g., inhomogeneities.

2. Results and Discussion

First, we introduce some definitions and discuss some general properties that determine the quadrupole splittings in HTSCs. We begin with the parent materials and denote the EFG at a nucleus by Ξ (we omit the label for O and Cu), a symmetric, traceless tensor with the three principal axis components ξ_{ii} , i.e.,

$$\Xi = (\xi_{11}, \xi_{22}, \xi_{33}) = \xi_{33} \left(-\frac{1}{2}(1 - \eta_\xi), -\frac{1}{2}(1 + \eta_\xi), 1 \right). \quad (1)$$

The asymmetry parameter η_ξ is given by,

$$\eta_\xi = \frac{\xi_{11} - \xi_{22}}{\xi_{33}}, \quad (2)$$

with the usual definition that ξ_{33} has the largest magnitude, i.e., $|\xi_{33}| \geq |\xi_{22}| \geq |\xi_{11}|$ ($\sum \xi_{ii} = 0$).

Based on symmetry arguments, one expects for the parent compound an EFG at planar Cu (in square planar arrangement with planar O) that is axially symmetric ($\eta_\xi = 0$). Since there is a substantial hole content in the Cu $3d(x^2 - y^2)$ orbital, a large quadrupole splitting, i.e., a large ξ_{33} , is expected ($\xi_{22} = \xi_{11} = -\xi_{33}/2$; note that we cannot determine the sign of the ξ_{ii} , hence we take ξ_{33} to be positive). One expects the principle axis of ξ_{33} to coincide with the crystal c-axis, i.e., it is perpendicular to the CuO_2 plane. The charges in Cu $3d(z^2 - r^2)$ or $4p$ orbitals do not affect the local Cu symmetry ($4s$ will not contribute to the EFG, at all). The situation is expected to be different at planar O, which is in an almost full shell configuration (for a full shell the EFG is zero). Therefore, one expects a small quadrupole splitting with its largest principle component along the $2p_\sigma$ bond due to hybridization of Cu $3d(x^2 - y^2)$ and O $2p_\sigma$ orbitals[9]. The asymmetry of the tensor is expected to be substantial since the two axes perpendicular to the O $2p_\sigma$ bond are not equivalent.

Doping the parent compounds must change the Cu and/or O EFGs, but will not change the fundamental local symmetry at either nuclear site. In the most simple

scenario one may assume that hole doping (x) creates an additional electric field with an axially symmetric EFG (X),

$$X = (x_{11}, x_{22}, x_{33}), \quad X = x_{33} \left(-\frac{1}{2}, -\frac{1}{2}, 1 \right). \quad (3)$$

For Cu this is mandatory, but for O the other $2p$ orbitals might be affected by the doping, as well. In the experiment we measure the sum of both EFGs ($\Theta = \Xi + X$),

$$\Theta = \theta_{33} \left(-\frac{1}{2}(1 - \eta_\theta), -\frac{1}{2}(1 + \eta_\theta), 1 \right), \quad (4)$$

and with (3) and (1) we have,

$$\theta_{11} = -\frac{1}{2}\theta_{33} - \frac{1}{2}\xi_{33}\eta_\xi, \quad \theta_{22} = -\frac{1}{2}\theta_{33} + \frac{1}{2}\xi_{33}\eta_\xi, \quad \theta_{33} = \xi_{33} + x_{33} \quad (5)$$

$$\eta_\theta = \frac{\xi_{33}\eta_\xi}{\xi_{33} + x_{33}}. \quad (6)$$

One recognizes that,

$$\theta_{33}\eta_\theta = \xi_{33}\eta_\xi, \quad \text{i.e.,} \quad \theta_{11} - \theta_{22} = \xi_{11} - \xi_{22}, \quad (7)$$

and a symmetric contribution due to doping will not change the anisotropy given by the parent background EFG. Again, for Cu this is trivial and only $^{63}\theta_{33}$ will change with doping. For planar O one has to resort to the data collected in Tab. 1. They reveal two important things. Firstly, there is a steady increase of $^{17}\theta_{33}$ with doping, as well as an increase from one family to another if $T_{c,\max}$ of the family is also larger. Secondly, the anisotropy $^{17}\theta_{11} - ^{17}\theta_{22}$ is rather similar for all HTSCs, and there appear to be only two groups of materials that differ in this background anisotropy at a finer level.

In order to investigate the ^{17}O results further, we plot in Fig. 1 the dependence $\theta_{11}(x)$ vs. $\theta_{22}(x)$ for the data shown in Tab. 1. We note that with (7) we have,

$$\theta_{11}(x) = \theta_{22}(x) + \xi_{33}\eta_\xi \equiv \theta_{22}(x) + (\xi_{11} - \xi_{22}). \quad (8)$$

We recognize in Fig. 1 the two groups of materials, easily. The dashed lines with slope one, cf. (8), are guides to the eye. The doping dependence of La-214 fits the scenario that doping adds a symmetric tensor, only (this behavior is explained even quantitatively by the holes entering O $2p_\sigma$ orbitals almost entirely [9]). Y-123 and Y-124 have nearly the same anisotropy, but deviate somewhat from the doping trend (perhaps since the other O orbitals are affected by the doping to some extent). Interestingly, the points for Y-123, Y-124 appear towards higher doping if one follows the line for La-214, i.e., further doping La-214 could generate the same points. The second group of materials, appearing to the left in Fig. 1, seem to follow a similar trend as doping is concerned, but their anisotropy is clearly different. Note that these materials are much more anisotropic, but they also have the highest $T_{c,\max}$. To conclude, the data reveal that doping the different systems does not change the anisotropy substantially, and we can use $^{17}\theta_{33}$ as a good measure of the hole content at planar oxygen. This is in agreement with the well-established fact that $^{17}\theta_{33}$ is a linear function of x , but it suggests that the differences in $^{17}\theta_{33}$ between different families are largely due to a difference in the local planar oxygen hole content, as well.

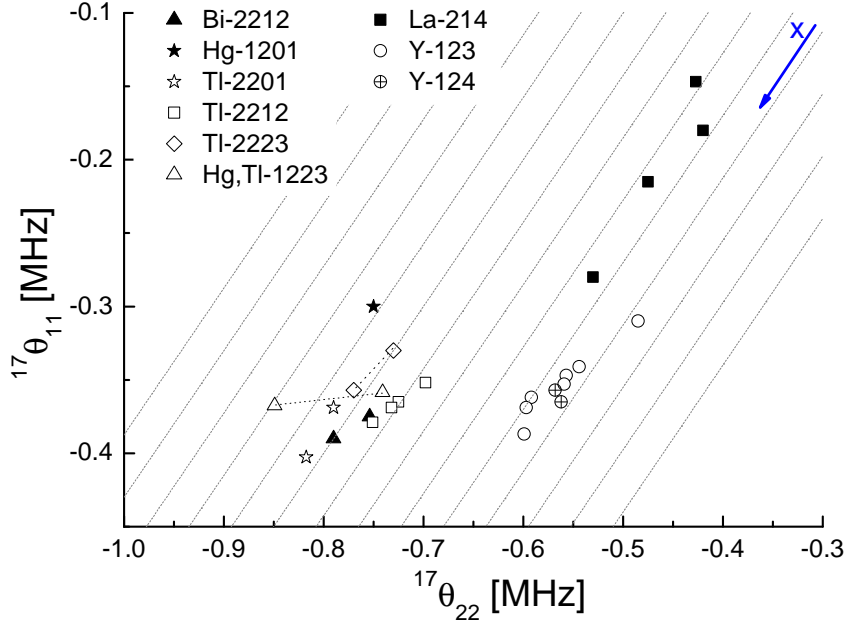


Figure 1. Components of the total planar ^{17}O EFGs of different cuprate families and doping levels from Tab. 1: $^{17}\theta_{11}$ (along the crystal c-axis) vs. $^{17}\theta_{22}$ (in the CuO_2 plane, perpendicular to $\text{O } 2p_\sigma$). The average doping (x) is known to be linear in $^{17}\theta_{33}$ ($= -^{17}\theta_{11} - ^{17}\theta_{22}$) and is indicated by the blue arrow. The data points for TI-2223 and Hg,TI-1223 that are connected by dashed lines belong to the two different O sites (inner and outer CuO_2 layer) for the same average doping[10]. The thin slanting dashed lines indicate a slope of 1, cf. (8).

To further inquire about this conclusion, we plot in Fig. 2 the largest principle components for Cu and O against each other, i.e., $^{63}\theta_{33}$ vs. $^{17}\theta_{33}$. We identify three groups of materials, now. First, we have La-214 with the largest $^{63}\theta_{33}$ and comparably small $^{17}\theta_{33}$ that strongly increases with doping (the holes enter the $\text{O } 2p_\sigma$ bond). The second group concerns the Y-123 data. The parent material of Y-123 starts at considerably lower $^{63}\theta_{33}$, but higher $^{17}\theta_{33}$; doping increases both parameters steadily. Interestingly, the stoichiometric Y-124 fits the set of data points. The third group of materials concerns those families that have the largest $T_{c,\text{max}}$. Unfortunately, we do not have data for their parent materials, however, they must lie at much smaller $^{63}\theta_{33}$ and considerably larger $^{17}\theta_{33}$. Doping appears to increase both values, similar to what is observed for the other systems.

Note, that a smaller Cu splitting ($^{63}\theta_{33}$) together with a larger O splitting ($^{17}\theta_{33}$) for a fixed total doping signals that the Cu hole has in part been transferred to planar O. In fact, we added a set of parallel lines from [9] representing constant doping. These lines support this scenario even quantitatively. Based on all the data one would argue that the planar O hole content is much higher in those systems that have the largest

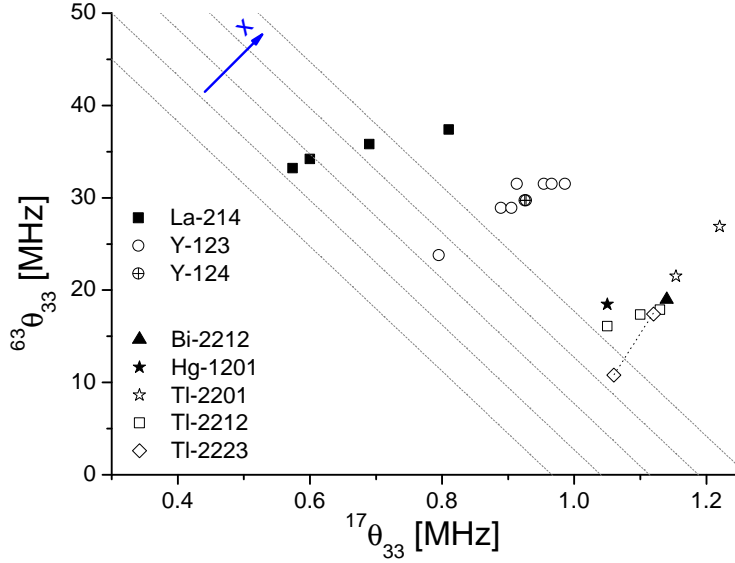


Figure 2. The largest EFG component at planar Cu ($^{63}\theta_{33}$) and O ($^{17}\theta_{33}$) plotted against each other (data from Tab. 1 and 2). The increase of the average doping is indicated by the blue arrow. The data points for Tl-2223 that are connected by a dashed line belong to the same doping level, but the two planar oxygen and copper sites from the inner and outer CuO_2 layers [10]. The slope of the thin, parallel lines follows from ref. [9] for fixed doping (e.g., $x=\text{const.}$).

$T_{c,\text{max}}$.

It is of course intriguing to plot the oxygen splitting that represents the number of O $2p_\sigma$ holes against the critical temperature for all materials. This "phase diagram" is shown in Fig. 3. Due to the lack of data away from optimal doping for some materials we do not have the full parabolic behavior of T_c on $^{17}\theta_{33}$ for all systems. Contrary to the typical phase diagram of the cuprates Fig. 3 suggests that there should be an offset between parabolas since the systems that can reach higher T_c do have a larger O $2p_\sigma$ hole content. We note that the values for $T_{c,\text{max}}$ do scale with $^{17}\theta_{33}$. This is true irrespective of the kind of doping (and therefore of issues of inhomogeneity). Doping a particular family to achieve the highest T_c does increase the planar O hole content further, but starting with a parent material that already has a higher planar O hole content is even more important. Doping only unlocks the highest possible T_c (by destroying the Cu based magnetism).

For Cu the number of available data is much larger, cf. Tab. 2, and we plot in Fig. 4 T_c vs. $^{63}\theta_{33}$ for the data we found in the literature. Clearly, there is the trend that materials with higher $T_{c,\text{max}}$ will be found at lower $^{63}\theta_{33}$, but the trend is perhaps less striking compared to the planar O data. However, the Cu parabolas reveal more clearly the dependence on doping. The absolute changes in the Cu splitting are much bigger than for oxygen so that the resolution is better, however, one has to be cautious

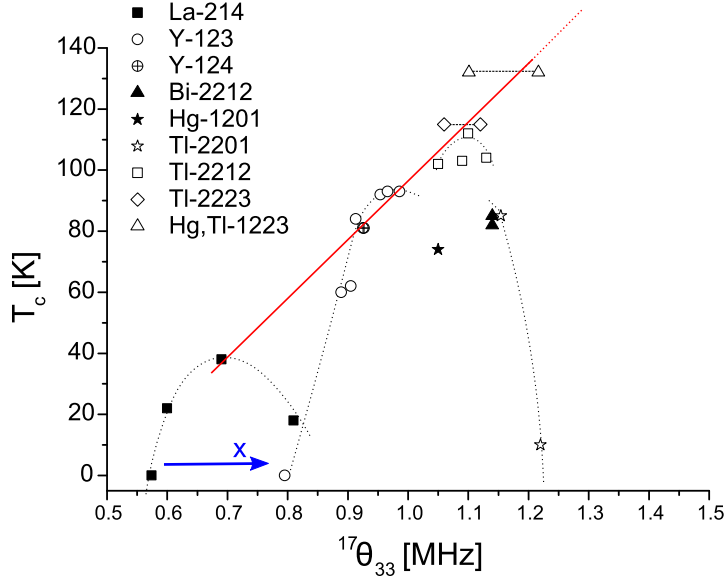


Figure 3. Phase diagram of the HTSCs based on ^{17}O NMR splittings (data from Tab. 1). The black dotted lines are guides to the eye and connect different doping levels for one family; for Tl-2223 and Hg,Tl-1223 connected pairs belong to the same average doping, but the different planar O sites. The red line approximately connects $T_{c,\text{max}}$. The blue arrow shows the increase of doping for all families.

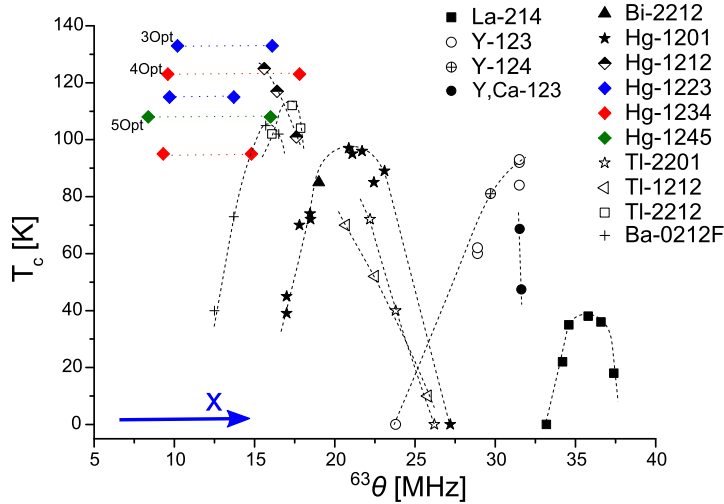


Figure 4. T_c versus the ^{63}Cu NMR splitting (data from Tab. 2). Black dashed lines are guides to the eye and connect different doping levels for one family (for the Hg-families with more than 3 CuO_2 layers the points are connected with colored dotted lines for the same average doping level). The blue arrow denotes the increase of the average doping for each family.

since $^{63}\theta_{33}$ depends also on the planar O hole content.[9]

To conclude, we have analyzed all data available to us for quadrupole splittings of planar Cu and O in the HTSCs. We find, as already stated in a number of publications,

that the largest principle EFG components for Cu ($^{63}\theta_{33}$) and O ($^{17}\theta_{33}$) are linear functions of the average doping (x). We then conclude that even the differences in $^{63}\theta_{33}$ and $^{17}\theta_{33}$ between different families are by and large based on the differences in the Cu vs. O hole content in the parent materials, i.e., for $x = 0$. We then show that the highest critical temperature ($T_{c,\text{max}}$) is a linear function of $^{17}\theta_{33}$, the planar oxygen hole content, i.e., the higher the oxygen hole content the higher $T_{c,\text{max}}$. This leads us to proposing a new phase diagram for the HTSCs. It has the planar oxygen splitting (and thus the planar oxygen hole content) as abscissa, as opposed to just x . In our phase diagram, the superconducting domes of families with different $T_{c,\text{max}}$ appear shifted, ordered with respect to the highest $T_{c,\text{max}}$. While doping increases T_c it is not the key factor in determining $T_{c,\text{max}}$. The proposed phase diagram might explain why one expects slight differences in the electronic properties for different families in the usual phase diagram.

Table 1. Principal values of the planar oxygen EFG for various cuprates and doping levels ("und." - underdoped, "opt." - close to optimal doping, "ovd." - overdoped). For Tl2223 and Hg,Tl-2223 there are two CuO_2 layers, the inner layer with O(1) and the outer layer O(2). Data are taken from: (a) Ref.[9], (b) Ref.[11], (c) Ref.[12], (d) Ref.[7], (e) Ref.[13], (f) Ref.[14], (g) Ref.[15], (h) Ref.[16], (i) Ref.[10], (j) Ref.[17].

Family	doping	T_c [K]	$^{17}\theta_{11}$ [MHz]	$^{17}\theta_{33}$ [MHz]	$^{17}\theta_{22}$ [MHz]	$^{17}\eta$ [MHz]	$^{17}\theta_{11} - ^{17}\theta_{22}$ [MHz]
La-214 ^a	0	0	-0.147	0.574	-0.427	0.488	0.280
	0.075	22	-0.18	0.6	-0.42	0.400	0.240
	0.15	38	-0.215	0.69	-0.475	0.377	0.260
	0.24	18	-0.28	0.81	-0.53	0.309	0.250
Y-123 ^a	0	0	-0.31	0.795	-0.485	0.220	0.175
	0.6	60	-0.341	0.889	-0.544	0.228	0.203
	0.63	62	-0.347	0.905	-0.557	0.232	0.210
	0.8	84	-0.353	0.913	-0.559	0.226	0.206
	0.96	92	-0.362	0.954	-0.592	0.241	0.230
	1	93	-0.387	0.986	-0.599	0.215	0.212
	1	93	-0.369	0.966	-0.597	0.236	0.228
Y-124 ^a		81	-0.365	0.927	-0.562	0.213	0.197
		81	-0.357	0.925	-0.568	0.228	0.211
Hg-1201 ^b		74 (und)	-0.300	1.050	-0.750	0.429	0.450
Tl-2201 ^{c,d}		85 (opt)	-0.369	1.154	-0.790	0.365	0.421
		10 (ovd)	-0.403	1.220	-0.817	0.340	0.415
Bi-2212 ^{e,f}		86 (opt)	-0.39	1.14	-0.75	0.316	0.360
		82 (ovd)	-0.375	1.140	-0.754	0.332	0.379
Tl-2212		103 (ovd) ^g	-0.365	1.09	-0.725	0.330	0.360
		102 (und) ^h	-0.352	1.05	-0.698	0.330	0.346
		112 (opt) ^h	-0.369	1.10	-0.732	0.330	0.363
		104 (ovd) ^h	-0.379	1.13	-0.751	0.330	0.372
Tl-2223 O(1) O(2)		115 (ovd?) ⁱ	-0.33	1.06	-0.73	0.377	0.400
			-0.357	1.12	-0.77	0.369	0.413
Hg,Tl-1223 O(1) outer O(2)		132 (opt) ^j	-0.359	1.101	-0.741	0.347	0.383
			-0.368	1.217	-0.849	0.396	0.482

3. Acknowledgments

We would like to thank O.K. Andersen, A. Bussmann-Holder, G. V. M. Williams, A. Erb, Th. Meier, R. Gühne, and O. P. Sushkov for helpful discussions. We also acknowledge financial support by Leipzig University, the DFG within the Graduate School Build-MoNa, the European Social Fund (ESF) and the Free State of Saxony.

Table 2. Principal values of the planar Cu EFGs for various cuprates and doping levels ("und." - underdoped, "opt." - close to optimal doping, "ovd." - overdoped) . For Tl- and Hg- families with more than 3 CuO_2 layers there are two Cu sites, the inner layer with Cu(1) and the outer layer Cu(2). Data are taken from: (a) Ref.[9], (aa) Ref.[18], (b) Ref.[19], (c) Ref.[20], (d) Ref.[21], (e) Ref.[22], (f) Ref.[23], (g) Ref.[24], (h) Ref.[25], (i) Ref.[26], (j) Ref.[27], (k) Ref.[28], (l) Ref.[29], (m) Ref.[30],

Family	T_c [K]	$^{63}\theta_{33}$ [MHz]
La-214 ^a	0	33.2
	22	34.2
	35	34.6
	38	35.8
	36	36.6
	18	37.4
Y-123 ^a	0	23.8
	60	28.9
	62	28.9
	84	31.5
	92	31.5
	93	31.5
Y-124 ^a	81	29.72
Y,Ca-123	68 (ovd) ^{aa}	31.55
	48 (ovd) ^{aa}	31.65
Hg-1201	39 (und) ^b	17.0
	45 (und) ^c	17.0
	70 (und) ^b	17.8
	72 (und) ^b	18.5
	74 (und) ^d	18.46
	95 (opt) ^b	21.1
	96 (opt) ^b	21.7
	97 (opt) ^e	20.88
	89 (ovd) ^b	23.1
	85 (ovd) ^c	22.4
	0 (ovd) ^b	27.2
Hg-1212	125 (opt) ^f	15.6
	117 (ovd) ^f	16.4
	101 (ovd) ^g	17.0
	101 (ovd) ^h	17.6
Hg-1223 Cu(1)	115 (und) ⁱ	9.7
	Cu(2)	13.7
----- Cu(1)	133 (opt) ^j	10.2
	Cu(2)	16.1
----- Hg,Cu-1223 Cu(1)	134 (opt) ^k	15.3
	Cu(2)	16.6
Hg-1234 Cu(1)	85 (und) ^l	9.3
	Cu(2)	14.8
----- Cu(1)	123 (opt) ^l	9.6
	Cu(2)	17.8
Hg-1245 Cu(1)	108 (opt) ^m	8.37
	Cu(2)	16

Table 3. ctd of Tab. 2, (n) Ref.[31], (o) Ref.[32], (p) Ref.[33], (r) Ref.[16], (s) Ref.[34], (t) Ref.[10], (u) Ref.[35].

Family	T_c [K]	$^{63}\theta_{33}$ [MHz]
Bi-2212	86 (opt) ⁿ	19.0
Tl-2201	72 (ovd) ^o	22.2
	40 (ovd) ^o	23.8
	0 (ovd) ^o	26.2
Tl-1212	70 (ovd) ^p	20.7
	52 (ovd) ^p	22.5
	10 (ovd) ^p	25.8
Tl-2212	102 (und) ^r	16.08
	112 (opt) ^r	17.35
	104 (ovd) ^r	17.87
Tl-2223 Cu(1)	125 (opt) ^s	11.7
Cu(2)		16.4
Cu(1)	115 (ovd?) ^t	10.8
Cu(2)		17.4
Ba-0212F	40 (und) ^u	12.5
	73 (und) ^u	13.7
	105 (opt) ^u	15.7
	102 (ovd) ^u	16.5

References

- [1] C. P. Slichter. Magnetic Resonance Studies of High Temperature Superconductors. In J.R. Schrieffer, editor, *Handbook of High-Temperature Superconductivity*. Springer, 2007.
- [2] L. C. Hebel and C. P. Slichter. Nuclear relaxation in superconducting aluminum. *Phys. Rev.*, 107:901, 1957.
- [3] J. Haase, C.P. Slichter, and G.V.M. Williams. Evidence for two electronic components in high-temperature superconductivity from NMR. *J. Phys.: Condens. Matter*, 21:455702, 2009.
- [4] J. Haase, D. Rybicki, C.P. Slichter, M. Greven, G. Yu, Y. Li, and X. Zhao. Two-component uniform spin susceptibility of superconducting $\text{HgBa}_2\text{CuO}_{4+\delta}$ single crystals measured using ^{63}Cu and ^{199}Hg nuclear magnetic resonance. *Phys. Rev. B*, 85:104517, 2012.
- [5] T. Meissner, S.K. Goh, J. Haase, G.V.M. Williams, and P.B. Littlewood. High-pressure spin shifts in the pseudogap regime of superconducting $\text{YBa}_2\text{Cu}_4\text{O}_8$ as revealed by ^{17}O NMR. *Phys. Rev. B*, 83:220517, 2011.
- [6] C.P. Slichter. *Principles of magnetic resonance*. Springer, 1990.
- [7] G. Zheng, Y. Kitaoka, K. Ishida, and K. Asayama. Local Hole Distribution in the CuO_2 Plane of High- T_c Cu-Oxides Studied by Cu and Oxygen NQR/NMR. *J. Phys. Soc. Jpn.*, 64:2524, 1995.
- [8] K. Asayama, Y. Kitaoka, G. Zheng, and K. Ishida. NMR studies of high T_c superconductors. *Prog. Nucl. Magn. Res. Spec.*, 28:221, 1996.
- [9] J. Haase, O. P. Sushkov, P. Horsch, and G. V. M. Williams. Planar Cu and O hole densities in high- T_c cuprates determined with NMR. *Phys. Rev. B*, 69:094504, 2004.
- [10] G. Zheng, Yoshio Kitaoka, Kunisuke Asayama, K. Hamada, H. Yamauchi, and S. Tanaka. NMR study of local hole distribution, spin fluctuation and superconductivity in $\text{Tl}_2\text{Ba}_2\text{Ca}_2\text{Cu}_3\text{O}_{10}$. *Physica C*, 260:197, 1996.
- [11] A. M. Mounce, Sangwon Oh, Jeongseop A. Lee, W. P. Halperin, A. P. Reyes, P. L. Kuhns,

- M. K. Chan, C. Dorow, L. Ji, D. Xia, X. Zhao, and M. Greven. Absence of Static Loop-Current Magnetism at the Apical Oxygen Site in $\text{HgBa}_2\text{CuO}_{4+\delta}$ from NMR. *Phys. Rev. Lett.*, 111:187003, 2013.
- [12] S. Kambe, H. Yasuoka, A. Hayashi, and Y. Ueda. NMR study of the spin dynamics in $\text{Tl}_2\text{Ba}_2\text{CuO}_y$ ($T_c=85\text{ K}$). *Phys. Rev. B*, 47:2825, 1993.
- [13] M. Takigawa and D. B. Mitzi. NMR Studies of Spin Excitations in Superconducting $\text{Bi}_2\text{Sr}_2\text{CaCu}_2\text{O}_{8+\delta}$ Single Crystals. *Phys. Rev. Lett.*, 73:1287, 1994.
- [14] J. Crocker, A. P. Dioguardi, N. Roberts-Warren, A. C. Shockley, H.-J. Grafe, Z. Xu, J. Wen, G. Gu, and N. J. Curro. NMR studies of pseudogap and electronic inhomogeneity in $\text{Bi}_2\text{Sr}_2\text{CaCu}_2\text{O}_{8+\delta}$. *Phys. Rev. B*, 84:224502, 2011.
- [15] A. Trokiner, K. Mikhalev, A. Yakubovskii, P.-V. Bellot, S. Verkhovskii, Yu. Zhdanov, Yu. Piskunov, L. Shustov, A. Inyushkin, and A. Taldenkov. ^{17}O NMR in high- T_c superconductor $\text{Tl}_2\text{Ba}_2\text{CaCu}_2\text{O}_y$. *Physica C*, 255:204, 1995.
- [16] A. Gerashenko, Yu. Piskunov, K. Mikhalev, A. Ananyev, K. Okulova, S. Verkhovskii, A. Yakubovskii, L. Shustov, and A. Trokiner. The ^{63}Cu and ^{17}O NMR studies of spin susceptibility in differently doped $\text{Tl}_2\text{Ba}_2\text{CaCu}_2\text{O}_{8-\delta}$ compounds. *Physica C*, 328:163, 1999.
- [17] K.H. Lim, H.C. Lee, and N.H. Hur. An ^{17}O NMR study of $\text{Hg}_{0.5}\text{Tl}_{0.5}\text{Ba}_2(\text{Ca}_{1-x}\text{Sr}_x)_2\text{Cu}_3\text{O}_{8+\delta}$. *Physica C*, 232:215, 1994.
- [18] G. V. M. Williams, S. Kramer, and M. Mehring. Nuclear-quadrupole-resonance study of overdoped $\text{Y}_{1-x}\text{Ca}_x\text{Ba}_2\text{Cu}_3\text{O}_7$. *Phys. Rev. B*, 63:104514, 2001.
- [19] A. A. Gippius, E. V. Antipov, W. Hoffmann, and K. Luders. Nuclear quadrupole interactions and charge localization in $\text{HgBa}_2\text{CuO}_{4+\delta}$ with different oxygen content. *Physica C*, 276:57, 1997.
- [20] D. Rybicki et. al. unpublished.
- [21] D. Rybicki, J. Haase, M. Lux, M. Jurkutat, M. Greven, G. Yu, Y. Li, and X. Zhao. ^{63}Cu and ^{199}Hg NMR study of $\text{HgBa}_2\text{CuO}_{4+\delta}$ single crystals. *arXiv:1208.4690*, 2012.
- [22] D. Rybicki, J. Haase, M. Greven, G. Yu, Y. Li, Y. Cho, and X. Zhao. Spatial Inhomogeneities in Single-Crystal $\text{HgBa}_2\text{CuO}_{4+\delta}$ from ^{63}Cu NMR Spin and Quadrupole Shifts. *J. Supercond. Nov. Magn.*, 22:179, 2009.
- [23] S. Ohsugi, T. Tsuchiya, T. Koyama, and K. Fueki. Gapless superconductivity in overdoped Hg System; Cu-NQR study. *J. Low Temp. Phys.*, 105:419, 1996.
- [24] M. Horvatic, C. Berthier, P. Carretta, J.A. Gillet, P. Sgransan, Y. Berthier, and J.J. Capponi. NMR investigation of $\text{HgBa}_2\text{CaCu}_2\text{O}_{6+\delta}$. *Physica C*, 235:1669, 1994.
- [25] M.-H. Julien, M. Horvatic, P. Carretta, C. Berthier, Y. Berthier, P. Segransan, S.M. Loureiro, and J.-J. Capponi. ^{63}Cu and ^{199}Hg NMR in overdoped $\text{HgBa}_2\text{CaCu}_2\text{O}_{6+\delta}$. *Physica C*, 268:197, 1996.
- [26] M.-H. Julien, M. Horvatic, C. Berthier, and P. Segransan. ^{63}Cu NMR in the normal state of $\text{HgBa}_2\text{Ca}_2\text{Cu}_3\text{O}_{8+\delta}$. *J. Low Temp. Phys.*, 105:371, 1996.
- [27] K. Magishi, Y. Kitaoka, G.-q. Zheng, K. Asayama, K. Tokiwa, A. Iyo, and H. Ihara. ^{63}Cu NMR probe of superconducting properties in $\text{HgBa}_2\text{Ca}_2\text{Cu}_3\text{O}_{8+\delta}$: A possible reason for $T_c=133\text{ K}$. *Phys. Rev. B*, 53:R8906, 1996.
- [28] H. Breitzke, I. Eremin, D. Manske, E.V. Antipov, and K. Luders. Formation of magnetic moments in the cuprate superconductor $\text{Hg}_{0.8}\text{Cu}_{0.2}\text{Ba}_2\text{Ca}_2\text{Cu}_3\text{O}_{8+\delta}$ below T_c seen by NQR. *Physica C*, 406:27, 2004.
- [29] K. Itohara, S. Shimizu, H. Mukuda, Y. Kitaoka, P. M. Shirage, H. Kito, and A. Iyo. Number of CuO_2 layers dependence of magnetic quantum criticality in homogeneously doped high- T_c copper oxides: A ^{63}Cu -NMR study on four-layered high- compounds $\text{HgBa}_2\text{Ca}_3\text{Cu}_4\text{O}_{8+y}$. *Physica C*, 470:S140, 2010.
- [30] H. Kotegawa, Y. Tokunaga, Y. Araki, G.-q. Zheng, Y. Kitaoka, K. Tokiwa, K. Ito, T. Watanabe, A. Iyo, Y. Tanaka, and H. Ihara. Coexistence of superconductivity and antiferromagnetism in multilayered high- T_c superconductor $\text{HgBa}_2\text{Ca}_4\text{Cu}_5\text{O}_y$: Cu-NMR study. *Phys. Rev. B*, 69:014501, 2004.

- [31] K. Ishida, Y. Kitaoka, K. Asayama, K. Kadowaki, and T. Mochiku. Cu NMR Study in Single Crystal $\text{Bi}_2\text{Sr}_2\text{CaCu}_2\text{O}_8$ Observation of Gapless Superconductivity. *J. Phys. Soc. Jpn.*, 63:1104, 1994.
- [32] K. Fujiwara, Y. Kitaoka, K. Ishida, K. Asayama, Y. Shimakawa, T. Manako, and Y. Kubo. NMR and NQR studies of superconductivity in heavily doped $\text{Tl}_2\text{Ba}_2\text{CuO}_{6+y}$ with a single CuO_2 plane. *Physica C*, 184:207, 1991.
- [33] K. Magishi, Y. Kitaoka, G.-q. Zheng, K. Asayama, T. Kondo, Y. Shimakawa, T. Manako, and Y. Kubo. Magnetic excitation and superconductivity in overdoped $\text{TlSr}_2\text{CaCu}_2\text{O}_{7-\delta}$: A ^{63}Cu NMR study. *Phys. Rev. B*, 54:10131, 1996.
- [34] Z.P. Han, R. Dupree, R.S. Liu, and P.P. Edwards. ^{63}Cu NMR shift and relaxation behavior in $\text{Tl}_2\text{Ba}_2\text{Ca}_2\text{Cu}_3\text{O}_{10-\delta}$ ($T_c=125\text{K}$). *Physica C*, 226:106, 1994.
- [35] S. Shimizu, S. Iwai, S. Tabata, H. Mukuda, Y. Kitaoka, P. M. Shirage, H. Kito, and A. Iyo. Planar CuO_2 hole density in high- T_c cuprates determined by NMR Knight shift: ^{63}Cu NMR on bilayered $\text{Ba}_2\text{CaCu}_2\text{O}_4(\text{F},\text{O})_2$ and three-layered $\text{Ba}_2\text{Ca}_2\text{Cu}_3\text{O}_6(\text{F},\text{O})_2$. *Phys. Rev. B*, 83:144523, 2011.